Specular baffle for improved infrared integrating sphere performance.

L. M. Hanssen, A. V. Prokhorov and V. Khromchenko
Optical Technology Division, NIST, 100 Bureau Dr., Gaithersburg, MD 20899-8442

ABSTRACT

Baffles are often placed in integrating spheres to accommodate the non-ideal aspects of other sphere components. These include detectors, sources, sphere wall surface shape and coatings. Baffles intentionally prevent light interchange between these and other important sphere components and regions such as entrance/exit ports, sample, reference and detector field-of-view. The challenge for an integrating sphere designer is to position and construct baffles that achieve the primary goal of shadowing specific elements from each other, while at the same time minimizing all other "side„ effects that the baffles may have. Perhaps the most important side effect is the additional signal loss for light arriving at or leaving the sample from or to the baffle due to its absorptance. This is especially true for coatings and spectral ranges where the wall reflectance is relatively low such as for $BaSO_4$ above 1.5 μm and diffuse gold. A potential improvement that we have investigated in an infrared reflectometer sphere is the use of a specular coating that has significantly higher reflectance than any other available diffuse coating. In our case we have used specular gold versus the diffuse gold-coated plasma-sprayed metal coating that is on the sphere wall. Although this provides for lower loss of light reflected from the sample onto the baffle, the side effects must also be considered and reduced in the design. Specifically one needs to consider the mirroring that will take place in the sphere. In this paper we discuss the important design issues along with some integrating sphere characterization results that demonstrate improved sphere performance by use of specular baffles.

Keywords: integrating sphere, reflectance, baffle, specular, diffuse, hemispherical.

1.   INTRODUCTION

NIST has established scales for infrared spectral reflectance and transmittance for both specular and diffuse (directional-hemispherical) samples. A custom designed integrating sphere is used for the primary absolute measurements. In addition, absolute measurement methods have been developed for both regular and directional-hemispherical reflectance and transmittance.[1-4] The method used for directional-hemispherical reflectance includes characterization of the throughput uniformity/variation of the sphere (with respect to the angular distribution of the sample reflected light). The characterization can also be used as a tool to evaluate the performance of the elements of the sphere and to understand how they interact with each other. This process has been applied to our integrating sphere and specifically to the baffles that are used to shade specific regions of the sphere from one another.

Baffles are a critical element of any integrating sphere design. Even the first integrating sphere depicted in a publication by Ulbricht,[5] built for the measurement of total luminous flux, makes use of a baffle. In reflectometers, baffles are typically used to prevent light reflected from the sample to directly illuminate the detector port or the detector field-of-view (FOV). This is done to reduce the uncertainty and measurement error associated with variation in the scattering characteristics of potential samples.[1] In almost all cases, baffles are diffuse, with coatings identical to those used for the integrating sphere wall. It is generally best to use the highest reflectance coating available in order to minimize absorption of light by the baffle and thereby minimize the perturbation caused by the baffle to the ideal perfect sphere. In the ultraviolet-visible-near-infrared spectral region the highest reflecting coatings are nearly Lambertian. However, at longer wavelengths the sphere wall coatings available are various gold-coated rough surfaces. These all exhibit reflectance that is high for infrared diffusers, but nevertheless significantly lower than their UV-vis-NIR counterparts.

2. INFRARED INTEGRATING SPHERE AND BAFFLE PERFORMANCE

A schematic of our infrared integrating sphere is shown in Figure 1. The input beams for the sample and reference measurements for reflectance are shown, along with the locations of light first striking the sphere wall for the specular sample case.

The sphere has four baffles: (1 & 2) primary baffles between the sample (and reference) and the FOV of the detector, less critical baffles (3) between the sample (and reference) and the detector port and (4) between the sample and reference ports. The original construction of the sphere included three sets of interchangeable baffles: (i) diffuse baffles with the same coating as the sphere wall (an electroplated gold on top of plasma-sprayed copper); (ii) specular baffles with electroplated gold, and (iii) no baffles (diffuse plugs to fill the small ports used to mount the baffles). Three options were constructed for flexibility and sphere evaluation. The "standard,, diffuse baffle case for conventional sphere operation, the specular baffle case for potentially more uniform sphere throughput, and the "no baffle,, case which allows one to have a nearly complete spherical surface (with the use of port covers curved to match the sphere surface) without the perturbation of interior baffles. The last case enables one to perform measurements with and without port covers to obtain the hemispherical reflectance of the sphere wall according to one of Taylor's absolute methods.[3]
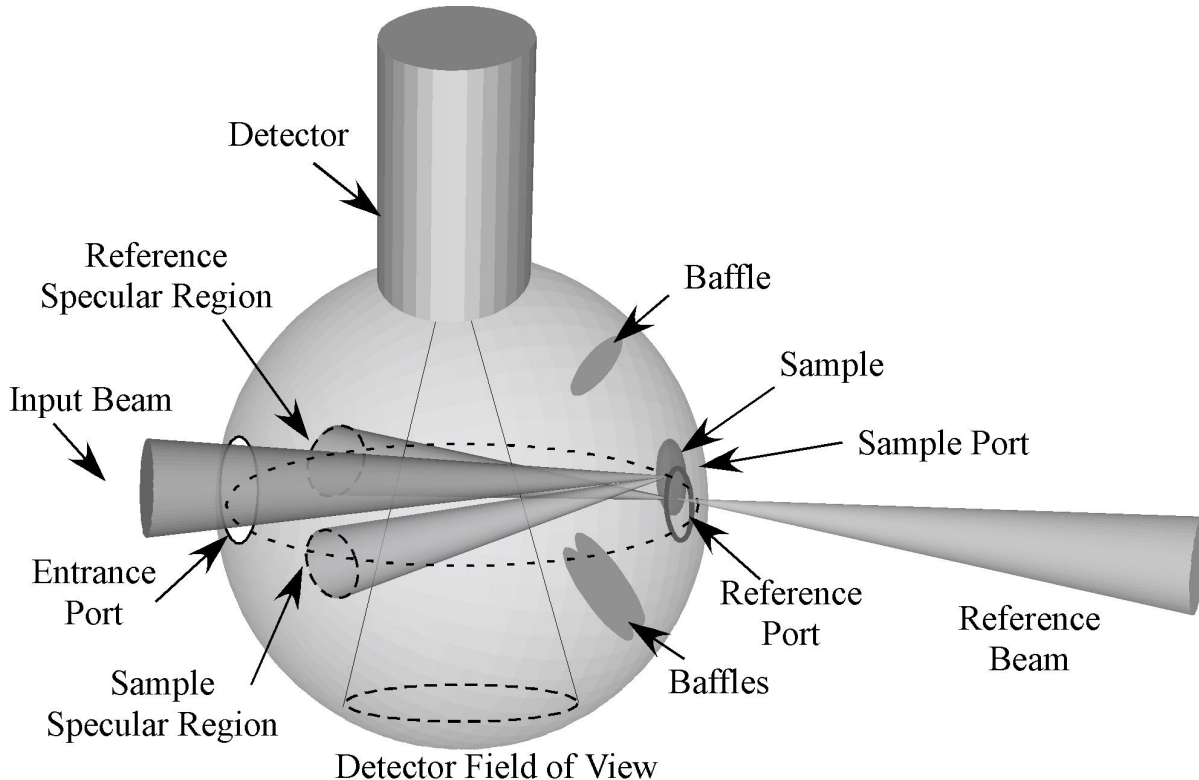

Figure 1. Integrating sphere schematic showing key components of sphere and measurement scheme for reflectance measurements, including baffles and input beams for sample and reference measurements that are incident on the sample specular region (for specular samples) and reference specular region (empty reference port), respectively. Baffle between sample and reference ports not shown.

As described in Reference 2, a measurement of this same sphere throughput variation (sphere mapping) was performed using a CO_2 laser source operating at 10.6 μm. The results of the mapping evaluation are shown in Figure 2. The "no baffles,, case curve shows why the baffles are required: for light directed into the FOV, the signal is as much as 2.5

times greater than that directed out of the FOV. The difference in strengths of these signals is directly related to the size of the FOV and can be reduced by increasing the FOV, but is difficult to eliminate completely, especially for cryogenically cooled and windowed detectors.[6]
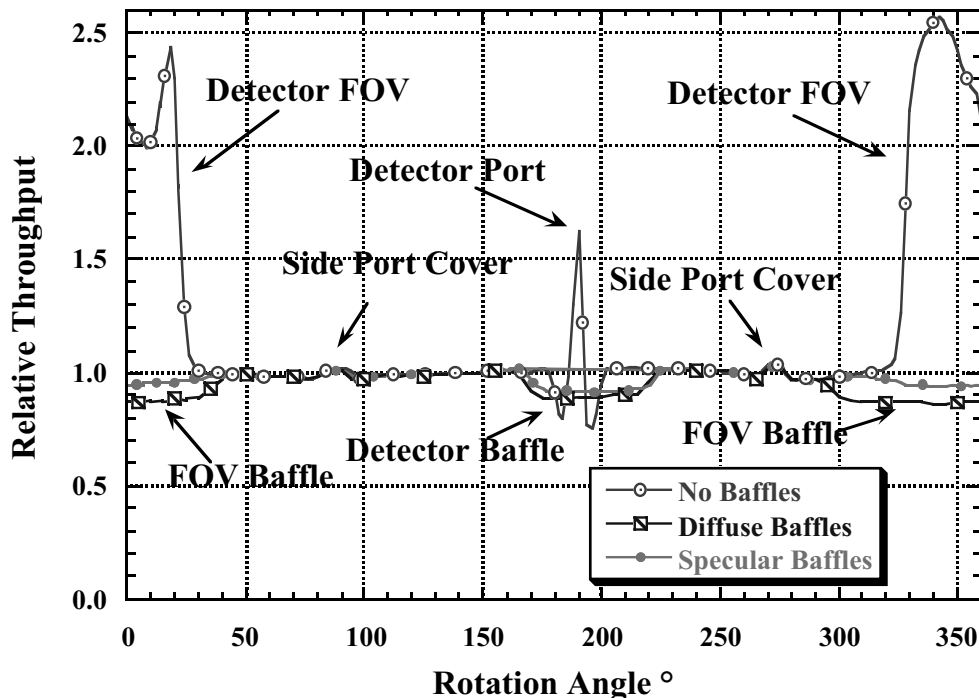

Figure 2. Comparison plot of the spatial uniformity scan of the integrating sphere measured at 10.6 μm. Results are shown for three different arrangements of the sphere: (a) with no baffles, (b) with specular baffles, and (c) with diffuse baffles. (Figure 6 from Reference 2.)

The need for a baffle between the sample (and reference) and the detector port is not so strong, because the non-imaging lens-concentrator design of the detector optics rejects almost all the light entering from outside the FOV.[7] However, due to a minor amount of leakage from secondary reflections in the lens, we have employed a baffle to reduce the maximum possible error due to a potential problem sample.

Finally, a clear improvement in the throughput uniformity can be seen for the specular baffles as compared to the diffuse baffles. These results would have led us to employ only the specular baffles for all future measurements, except that the scans of Figure 2 represent only one cross section of the sphere. And even though it is the most critical scan, one must consider the complete sphere map, which is shown in Figure 3.

The throughput maps shown in Figure 3 are for the (a) specular and (b) diffuse baffle cases, taken at 10.6 μm. The relative throughput range for both plots is from 0.8 to 1.1, and the sphere area covered in spherical coordinates is: polar angle (with 0 degrees at the center of the entrance port): 20 to 140 degrees in steps of 20, azimuthal angles: 0 to 360 degrees in steps of 5. The sample- and reference-FOV baffles can be clearly seen at the center top and bottom of each plot, as well as the sample and reference-detector baffle in the plot center. The small brighter points in between the baffles are due to the side port covers which have higher reflectance than the surrounding sphere wall. As in Figure 2, the diffuse baffle case shows greater non-uniformity than the specular baffle case over the entire map, except for one spot near the lower left corner in Figure 3(a). This spot for the specular baffle case represents a direct reflection into the detector port, for which the relative throughput is 3. Due to this large spike in the throughput, the specular baffles could not be used, yet their potential is clearly demonstrated by the comparison in Figure 3.
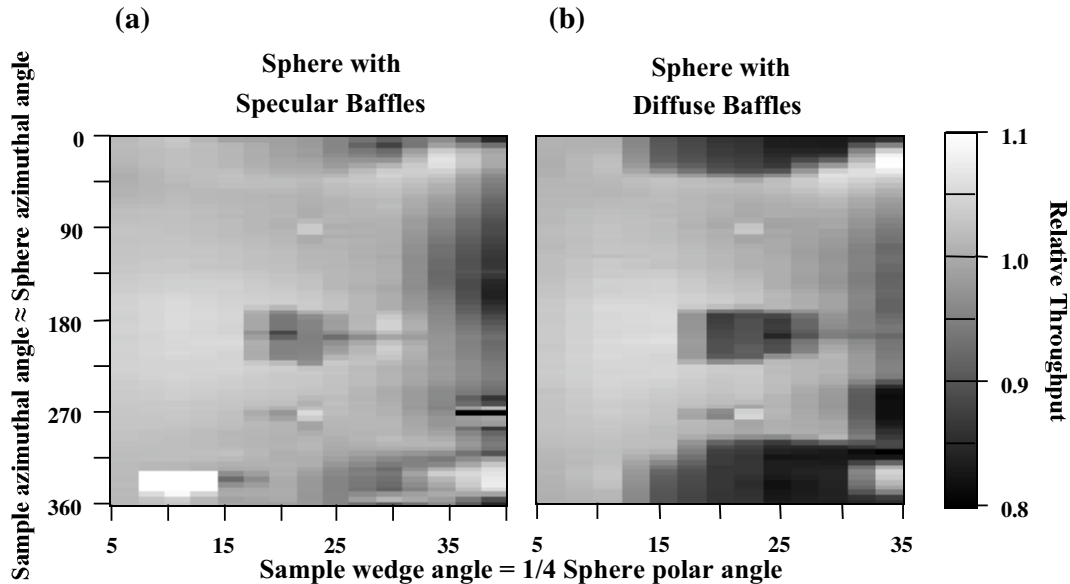
Figure 3. Comparison of the spatial uniformity mapping of the integrating sphere measured at 10.6 μm (a) with specular baffles, and (b) with diffuse baffles. The coverage of the sphere is complete except for the positions corresponding to the front (entrance port) and back (sample & reference ports) of the sphere (as viewed in Figure 1). The scale is shown by the bar on the far right. (Figure 7 from Reference 2])

3. BAFFLE DESIGN

To achieve the maximum potential of the use of specular baffles in an integrating sphere requires a careful design study. The design must meet a number of criteria that are shown schematically in Figures 4 and 5. First of all the baffle must perform it's primary shading task, preventing light directly reaching the detector FOV from the sample (reference), indicated in Figure 4 as "I,,. In addition, the baffle must not block any of the incident part of the beam from striking the sample, indicated by a "II,,. Finally, the baffle must not protrude into the detector's FOV, indicated as "III,,. These constraints apply to the baffle, whether it is diffuse or specular. Similar constraints apply to the baffle shading the detector port from the sample. However, the sphere design has a much larger FOV than detector port, so that the constraints on the FOV baffle are more restrictive and difficult to adhere to.

Additional constraints put on specular baffle designs are shown in Figure 5: the specular reflections by the baffle that need to be avoided. The reflections are denoted for the sample-to-FOV baffle. The light directed by the baffle into the detector port, found in the older specular baffle design, is labeled as (1). Additional reflections to be avoided are those directed via the baffle to the entrance port, reference port, and back onto the sample. For the sample-to-detector baffle, reflections should similarly avoid the FOV, entrance port, sample and reference, labeled as (6) in Figure 5. For the sample-to-reference baffle, back reflection to the sample or the entrance port should not occur. Finally, multiple reflections between baffles should also avoid these ports and regions.

Due to the 3 dimensional nature of the design, ray tracing is the best approach to analyze and refine the sizes and locations of the baffling in a sphere design. We are in the process of constructing a complete sphere model based on Monte-Carlo raytracing methods for comprehensive analysis of our infrared integrating sphere, similar in design to earlier work.[8]
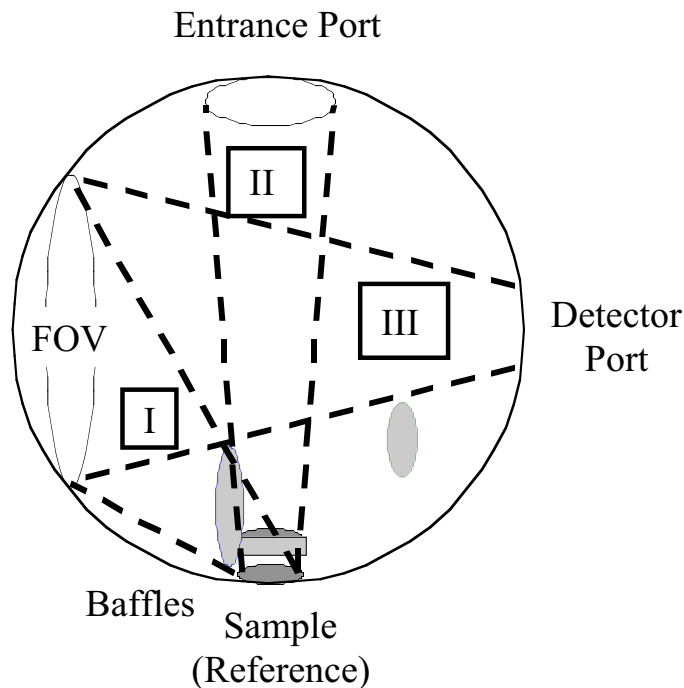
Figure 4. Requirements for primary baffle(s) design between the sample (and reference) and the FOV. First (I) the baffle must prevent light directly reaching the detector FOV from the sample (or reference). In addition, the baffle must not interfere with the (II) intput beam or (III) the detector view of its FOV. Similar restrictions are placed on the secondary baffles, but are easily adhered to.
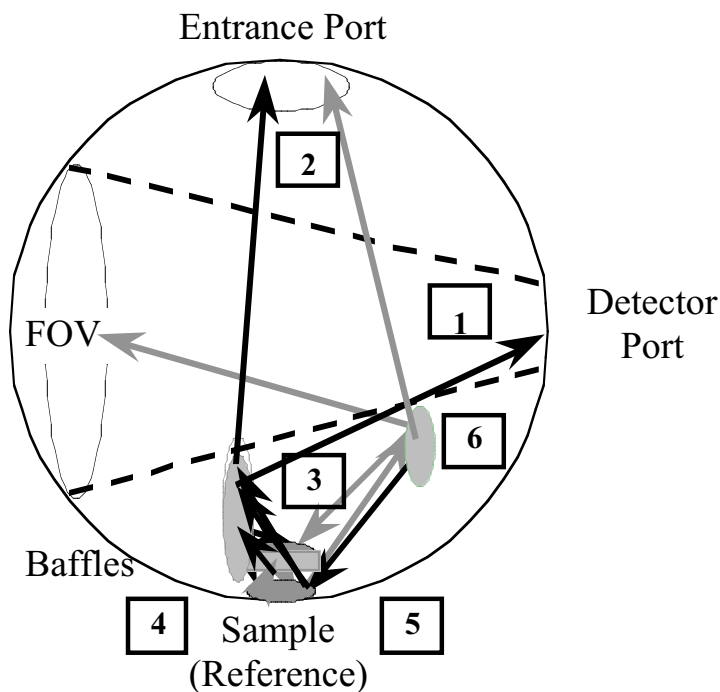

Figure 5. Additional design constraints for the use of specular baffles. The baffles should not reflect any light directly from the sample or reference to any of the following: via the primary baffle to (1) detector port, (2) entrance port, (3) reference port, (4) sample; via the baffle between the sample and reference (5) back onto the sample or reference; and (6) via the baffle between the sample and detector port to the FOV, entrance port, sample or reference.

We plan to study the effects of non-Lambertian sphere coatings and the secondary effects of non-imaging optics associated with the detector. However, for the purposes of the sizing and positioning of specular baffles, the first stage of the Monte Carlo program is sufficient. Output of the program is shown in Figure 6.
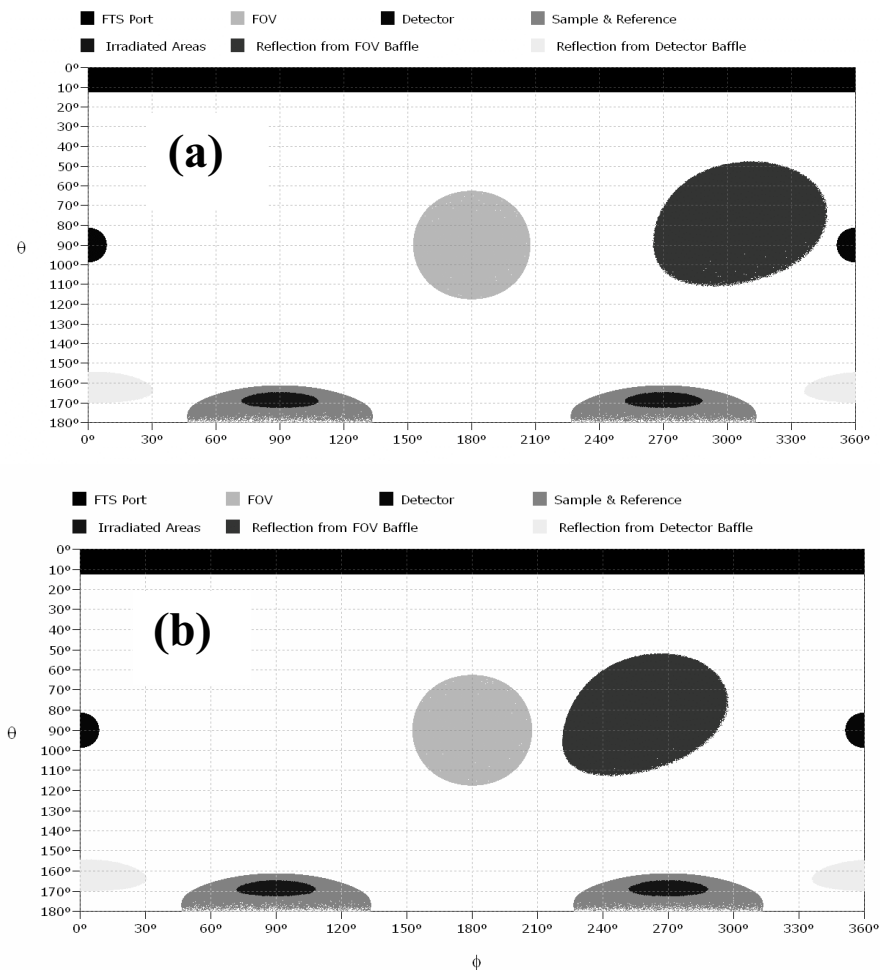

Figure 6. Examples of Monte Carlo raytrace output indicating location of specularly reflected light from a diffuse sample and specular baffles [spots to the right of center (off primary baffle) and split on right and left edges near the bottom (off sample/detector baffle)]. Also shown are the detector FOV (center), detector (split between right and left edges), sample and reference (on bottom) and entrance port (on top). The primary baffle in (a) is oriented in a way that its reflection is near the detector port, while in (b) it is closer to the FOV. In both cases, the baffle orientation is acceptable.

The plots in Figure 6 show the relative throughput for light directed over the sphere wall surface as a function of polar and azimuthal spherical coordinates. The coordinates are identical to those of Figure 3, except the azimuthal 0 includes the detector port center (as opposed to the FOV center in Figure 3). The plots show the locations of the detector, sample, reference, and entrance ports and the detector FOV, all entered by the user into the program. Since the sample and reference are under-illuminated, the maximum spot size is also shown. In addition, the user selects a coordinate value along the axis between the detector and the FOV, as well as two rotations about the other two orthogonal axes to define the plane of the baffle. The program then traces rays between the sample spot and the FOV to obtain the intesection of these rays with the baffle plane. These results provide the dimensions of the baffle required for

construction. After determining the intersection points, constraint (1) from Figure 4 is automatically satisfied. The program checks for compliance with constraints (2) and (3). Figure 6 (a) and (b) show the specularly reflected spots from the sample-FOV and sample-detector baffles for two different baffle orientations. In both (a) and (b) the reflected spots hit the sphere wall in an acceptable location. Other orientations not shown resulted in reflected spots overlapping with the other ports, as well as violation of constraints (2) and (3).

Based on the ray tracing results, baffles were constructed and installed in the sphere. A photo of the back half of the integrating sphere with baffles mounted is shown in Figure 7. The sample port has been reduced to the size of the maximum size input spot. The sample- and reference-detector baffles are combined into a single baffle seen near the top where half the detector port can also be seen. The sample- and reference-FOV baffles are tilted according to the ray-trace model design results.
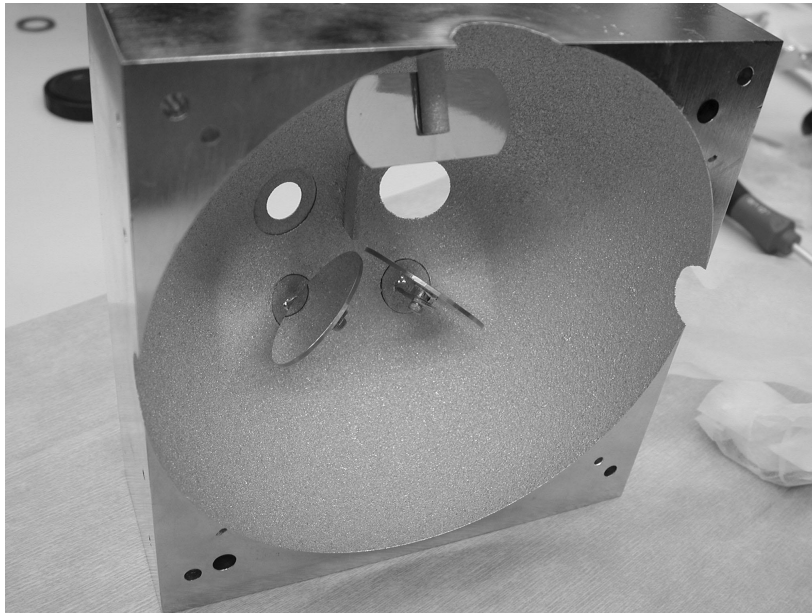

Figure 7. Photo of rear half of infrared integrating sphere, with specular baffles installed (except between sample and reference ports). The detector port is at the top of the sphere and the FOV region on the bottom. Side ports (generally covered when the sphere is assembled) can be seen on the edges.

4. NEW DESIGN PERFORMANCE

After installation of the specular baffles, the infrared integrating sphere was evaluated for two configurations: with both sample- and reference-FOV baffles installed, and with only the sample-FOV baffle installed. For almost all measurements performed with our sphere, since they are primarily absolute, as shown for reflectance in Figure 1, the reference port is almost always empty. When we use a reference, it is almost always specular (mirror or window). Hence, the primary shadowing required of the reference-FOV baffle is not required. Since it is generally best to minimize perturbations to the complete spherical shape, we have decided to operate with a single sample-FOV baffle. The tests performed on the sample/reference symmetry did not show any perceptible asymmetry as a result of the use of only one baffle. For other users who may wish to make relative measurements, the reference baffle should always be used. For the new design, the sample- reference-detector baffle has remained specular, and the sample-reference baffle has remained diffuse (to avoid a large back reflection component).

The first test of the sphere performance for the new specular baffle design is the measurement of a pressed powder polytetraflouroethylene (PTFE) sample. This material has been used as a standard for the visible and near infrared at NIST for many years and has been very well characterized.[9] Figure 8 shows a comparison of measurements of the PTFE sample made using the integrating sphere in both the older diffuse and new specular baffle designs, along with the standard values from Reference 9. The curves showing the measured results from our integrating sphere are uncorrected (simple ratio of sample to reference) prior to multiplication by a factor taking into account the sphere throughput variation according to our absolute reflectance method.
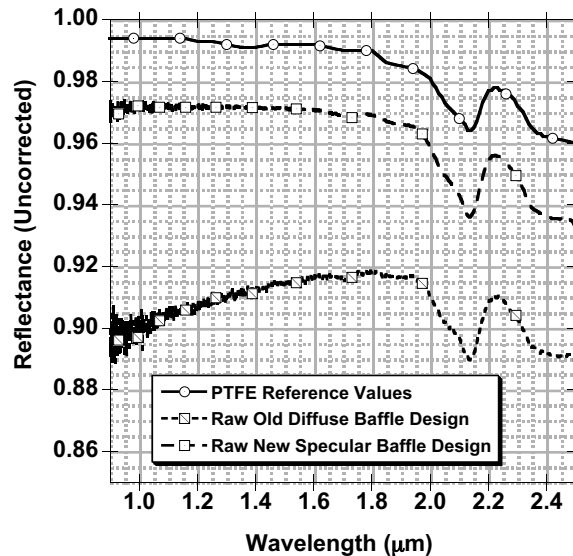

Figure 8. Comparison of reflectance measurements performed on pressed powder (PTFE), a high reflectance diffuse standard used for the visible and near infrared. The top curve is the calibrated hemispherical reflectance. The lower curve is the uncorrected ratio of sample to reference measurements using the previous sphere diffuse baffle design. The middle curve is the uncorrected ratio using the new sphere specular baffle arrangement.

The improvement in sphere performance is clearly demonstrated by the curves in Figure 8. The old diffuse baffle case results in a raw measurement from 4.5 % to 9 % below the actual hemispherical reflectance, whereas this is reduced to only 2.5 % for the new specular baffle design. It should be pointed out that even for a "perfect sphere,,, in this case one would expect a curve 1.2 % low due to the unavoidable loss of diffusely reflected light out the entrance port for a Lambertian sample. Hence the residual measurement error has been reduced by more than a factor of 3. Since the correction required for a specular sample is near 0 %, the uncertainty for an arbitrary sample with unknown scattering character for the new design will be in the 1.3 % to 2.5 % range as opposed to the 3.3 % to 9 % range before.

The second evaluation has been a new sphere throughput mapping performed across the entire spectral measurement range of 1 μm to 18 μm. The resulting map for 10 μm light is shown in Figure 9. This map is similar to that of Figure 3, except (a) the polar angle is 0 normal to the sample (near to, but not centered on the entrance port), (b) the azimuthal angle is the same as for Figure 6, and (c) the polar angle range is greater, from 0 to 160 deg.

The sample-FOV baffle can be near the center of the map. The entrance port is seen for polar angles 0 and 20 degrees and the throughput values integrate to approximately 1.2 % (as expected), The sample-FOV baffle is seen in the center on the plot. The two dark regions near the large polar angles correspond to (1) the post holding the sample-FOV baffle (narrow centered) and (2) the sample-reference baffle which is diffuse and unavoidably reflects light back onto the sample. A careful comparison of Figures 3 and 9 reveals better throughput uniformity for the new specular baffle design shown in Figure 9.
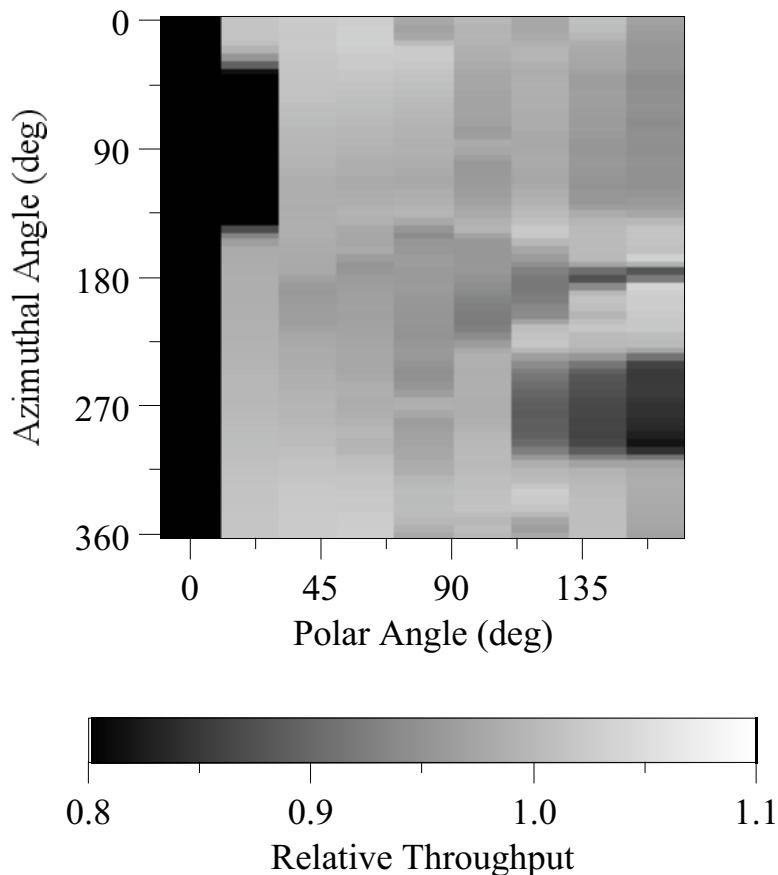
Figure 9. Sphere throughput map for new specular baffle design. This map covers the entire sphere, including azimuthal angle 0 and 160 degrees at the edges of the plot. The entrance port (not displayed in Figure 3) results in the black values below 0.8.

The two dark regions at large polar angles immediately suggest further improvements that might be made for the sphere. The baffle post could be remade to direct less light back towards the sample. Also, the flat diffuse sample-reference baffle could be replaced by a triangular cross-section specular baffle, to direct all the reflected light only onto the sphere wall.

5.   CONCLUSIONS

Baffles are critical to the optimum performance of integrating spheres, as well as their design including their arrangement and the positioning and sizing details. Specular baffles are shown to offer improved sphere performance over diffuse baffles for spheres with coatings designed for the infrared spectral region. This has been demonstrated through the results of sphere throughput mapping as well as by measurement of PTFE in the 1 μm to 2.5 μm range. However, careful evaluation of the mirroring effects of the baffles must be carried out. Ray tracing is well suited to perform the baffle optimization procedure. Replacement of the diffuse baffles separating the sample and reference from the detector field-of-view with specular baffles according to the optimized design in our infrared reflectance sphere has resulted in decreased uncertainties by a factor of 3 or better.

6. REFERENCES

1. K.A. Snail and L.M. Hanssen, "Integrating sphere designs with isotropic throughput,,, Appl. Opt. **28** (10), 1793-1799 (1989).
2. L.M. Hanssen and S.G. Kaplan, "Infrared diffuse reflectance instrumentation and standards at NIST,,, Analytica Chimica Acta **380**, 289-302 (1998).
3. L.M. Hanssen, "Integrating-sphere system and method for absolute measurement of transmittance, reflectance, and absorptance of specular samples,,, Appl. Opt. **40** (19), 3196-3204 (2001).
4. L.M Hanssen and K.A Snail, "Integrating spheres for mid- and near infrared reflection spectroscopy", in Handbook of Vibrational Spectroscopy, J.M. Chalmers and P.R. Griffiths (Eds), John Wiley & Sons, Ltd, Volume 2, pp. 1175 - 1192 (2002).
5. V.R. Ulbricht, "Die Bestimmung der mittleren räumlichen Lichtintensität durch nur eine Messung,,, Elektrotech. Zeit. **29**, 595-597 (1900).
6. L.M. Hanssen, "Effects of restricting the detector field of view when using integrating spheres,,, Appl. Opt. **28**, 2097 (1989).
7. D. Chenault, K.A. Snail, and L.M. Hanssen, "Improved integrating sphere throughput with a lens and nonimaging concentrator,,, Appl. Opt. **34**, 7959-7964 (Dec 1995).
8. A.V. Prokhorov and L.M. Hanssen, "Monte Carlo model of an integrating sphere reflectometer,,, Appl. Opt. **42**, 3832-3842 (2003).
9. V.R. Weidner, and J.J. Hsia, "Reflection properties of pressed polytetraflouroethylene powder,,, J. Opt. Soc. Am. **71**, 856-861 (1981).